AEM 2018

The effect of annealing conditions: temperature, time, ramping rate and atmosphere on nanocrystal Cu_2ZnSnS_4 (CZTS) thin film solar cell properties

Altowairqi, Y.[(1,2)] Alsubaie, A.[(2)] Stroh, K.P.[(1)] Perez-Marin, I.G.[(1)] Bowen, L.[(1)] Szablewski, M.[(1)] and Halliday, D.P.[(1)]

[(1)]Centre for Materials Physics, Department of Physics, Durham University, DH1 3LE, United Kingdom
[(2)]Department of Physics, Taif University, Saudi Arabia

Abstract

Cu_2ZnSnS_4 (CZTS) nanoparticles were fabricated successfully using the hot injection method; CZTS films were deposited by spin coating of nanocrystal ink. The aim of this work is to study the effect of annealing parameters: temperature, time, ramping rate and atmosphere on CZTS thin film structure and optical properties. XRD, Raman Spectroscopy, SEM, EDX mapping are used to analyse the films and they demonstrate the increase in quality and improvement in the crystallinity of CZTS and the homogeneity of elements which is one of the important factors for CZTS thin film solar cells. The crystallinity, structure and chemical composition of CZTS thin films increased and improved under annealing in H_2S+N_2 atmosphere which demonstrated that annealing at 500 ºC for 1 h with a ramping rate of 10 ºC/min under H_2S+N_2 atmosphere is a suitable condition for the fabrication of CZTS thin films used in solar cell devices.

1 Introduction

The annealing process is important for CZTS nanocrystal thin films to achieve high efficiency devices. However, controlling annealing parameters and their effects on CZTS device properties are still not well understood and still a current research question. Many studies have looked at these parameters. For instance, Wang et al. [1] studied the effect of temperature on CZTS films fabricated by evaporation, they found that annealing under high temperature

---

* Corresponding author. Douglas Halliday | Physics Department | Durham University | Durham | DH1 3LE | UK
  Email d.p.halliday@durham.ac.uk

leads to the film's surface decomposition but that it also increases the grain growth. Short annealing times also enhance throughput. It is well known that good crystallinity requires higher growth temperature, however, to avoid losing Sn during deposition, this needs be carried out at low temperature and followed by an increased temperature post deposition treatment to improve crystallinity [1, 2]. It was found that annealing of the CZTS film at 530 °C for 10 minutes in sulphur vapour eliminated all the secondary phases, and diffusion of sulphur in the film during the annealing process enhanced the crystallinity of the film [3]. Fukano at al. also studied the effect of the annealing process on CZTS electrical properties. The surface of CZTS thin films deposited by a sputtering technique which was followed by a sulfurisation process using a (5%) H_2S + (95%) N_2 atmosphere at 580 °C for different times of 10-60 minutes were analysed by scanning spreading resistance microscopy (SSRM). The spreading resistance (SR) was found to increase with increasing annealing time up to 30 minutes. This is probably caused by a decrease in the amount of point defects due to stabilization of the CZTS crystal grains. At 30 minutes the SR of the whole CZTS absorber layer becomes as large as the SR of the CdS buffer layer whereas for longer time periods close to 60 minutes the SR of the whole CZTS absorber layer becomes low, with the lowest SR areas being formed at the CZTS grain boundaries. This is probably caused by an increase in the carrier density induced by point defects in the CZTS crystals. The increased point defects are supposedly Cu substitutions at Zn sites, Cu_{Zn} antisite defects, which are dominant acceptors in p-type CZTS crystals which means that the SR is strongly dependent on the holding time of the sulfurisation [4]. The aim of the work reported in this study is to explore the effect of varying annealing parameters: temperature, time, ramping rate and atmosphere on CZTS thin films synthesised by the hot injection method and deposited by a spin coating approach by investigating crystal structure and optical properties.

2 Experimental Details

CZTS nanoparticles were prepared using the hot injection method [5, 6] as shown in Figure 1. The CZTS ink was deposited on a Mo layer on glass substrates using the spin coating technique.
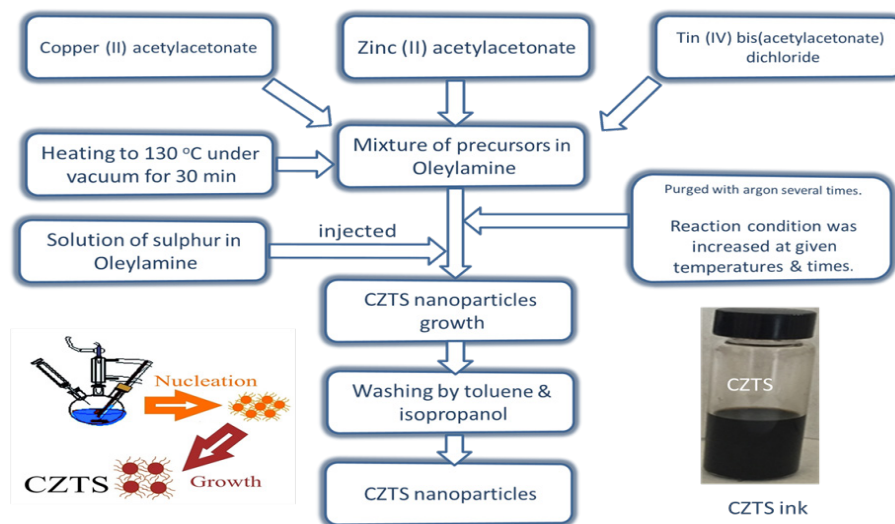

Figure 1 CZTS nanocrystal synthesis process.

The as-deposited precursor films were annealed at different annealing temperatures, times, ramping rates and in different atmospheres. The CZTS thin film substrates were loaded in a quartz tube furnace. For an N_2 atmosphere where different annealing temperature, time and ramping rate conditions were applied, the tube was evacuated using a rotary vacuum pump and the furnace tube subsequently filled with N_2 gas. For a H_2S atmosphere, after rotary pump evacuation, a gas mix of H_2S and N_2 with a composition ratio of 20:80 was introduced at a pressure of 0.15 atm. For

furnace annealing treatments, various temperatures, times and ramping rates were applied. The processes commenced at 300 °C with a ramping rate of 10 °C/min for 1 hour under N_2 atmosphere. After that the furnace was left to cool slowly overnight. These processes were repeated for different temperatures 400, 500 and 600 °C, and for different times 0.5, 1.5 and 2 hours, and different ramping rates 5, 15 and 20 °C/min. After annealing, the films were further characterized for their structural, morphological, compositional, and optical properties.

3 Results and Discussion

3.1 Annealing effect under different temperature

The X-ray diffraction patterns of the annealed CZTS films at various annealing temperatures are shown in Figure 2. The peaks located at 18.22°, 28.51°, 33.11°, 47.41°, 56.24° and 69.50° correspond to the characteristic (101), (112), (200), (220), (312) and (008) peaks of the kesterite structure (JCPDS card 26-0575). Also, there are other peaks at 27.50° in samples annealed at 300 °C and 400 °C. The peak at 40.61° in all samples corresponds to the Mo layer. However, peaks corresponding to the secondary phases SnS_2 at 33.02° (JCPDS card 83-1707), SnS at 45.80° (JCPDS card 83-1758) and Cu_3SnS_4 at 37.27°, 39.81°, 51.80° (JCPDS card 36-0217) are not observed [7, 8].
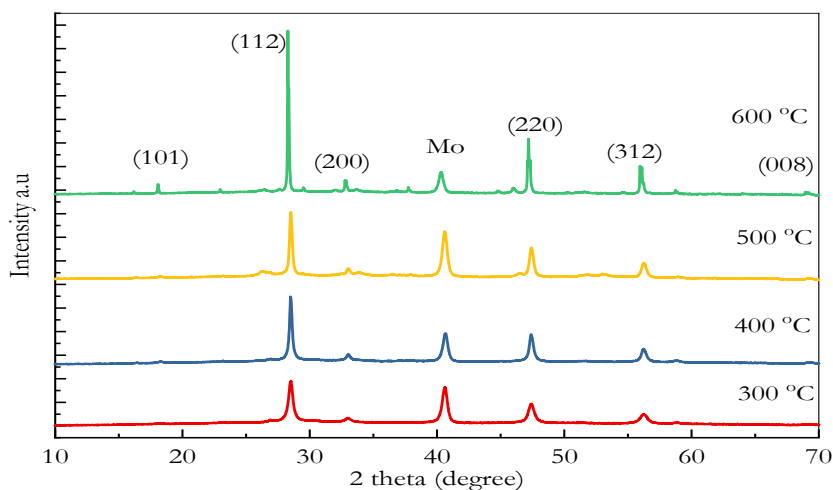

Figure 2 X-ray diffraction of CZTS films annealed at different temperatures 300, 400, 500 and 600 °C.

The grain size of the crystallites were calculated by using the Debye Sherrer's equation and found to be 42.25 nm, 68.32 nm, 70.71 nm and 291.49 nm for annealing temperatures of 300, 400, 500 and 600 °C, respectively. It is clear that the size of CZTS nanoparticles increases with increasing annealing temperature. The *d* spacing was calculated for the (112) and (220) planes and found to be 3.11 Å and 1.91 Å which agrees with previous literature reports [9-11] .

It is known that binary and ternary sulphides such as ZnS, $Cu_{2-x}S$ and Cu_2SnS_3 have similar x-ray peaks compared with CZTS. This can lead to difficulties in distinguishing those phases by x-ray diffraction. Raman spectroscopy provides unambiguous identification of these phases. The room temperature high resolution Raman spectra measurements of CZTS films annealed at different temperatures is shown in Figure 3. Peaks were fitted to this data confirming intense peaks at 338 cm⁻¹ for all annealing temperatures except the sample which was annealed at 400 °C which displayed an intense peak at 339 cm⁻¹.

However, the intense Raman peaks have an additional weak feature at lower wavenumbers at 334 cm⁻¹ for all samples except the sample which was annealed at 400 °C where this occurs at 337 cm⁻¹ [12]. For each sample, small peaks are formed in the shoulder located at different wavenumbers. For instance, in the sample annealed at 300 °C , the Raman

peaks are located at 257, 289, 356 and 360 cm^{-1}. In the sample annealed at 400 ^{o}C Raman peaks are found at 259, 288, 354 and 367 cm^{-1}, in the sample annealed at 500 ^{o}C Raman peaks are found at 253, 280, 287, 351 and 367 cm^{-1} and in the sample annealed at 600 ^{o}C, the Raman peaks located at 266, 287, 351 and 368 cm^{-1} which is associated with single phase CZTS. However, there is no evidence of secondary phases such as ZnS with a Raman peak at 350 cm^{-1}, $CuSnS_3$ with a peak at 320 cm^{-1} and $Sn_{2-x}S$ with a peak at 475 cm^{-1} expect for the sample annealed at 300 ^{o}C [13]. There are additional peaks at 313 cm^{-1} for the sample annealed at 600 ^{o}C and at 328 cm^{-1} for the sample annealed at 400 ^{o}C which corresponds to the CZTS phase [14-16]. Therefore, all major Raman peaks are attributed to different Raman modes in the CZTS kesterite structure. The peak centred at 338 cm^{-1} is attributed to the main A mode; a slightly red-shifted peak at 334 cm^{-1} that causes broadening of the main peak most likely represents the partially disordered kesterite phase (DKS) or Stannite phase, the peak centred at 287 cm^{-1} corresponds to the second A mode of kesterite, and the peak at 368 cm^{-1} can be attributed to E modes of CTZS [17, 18].
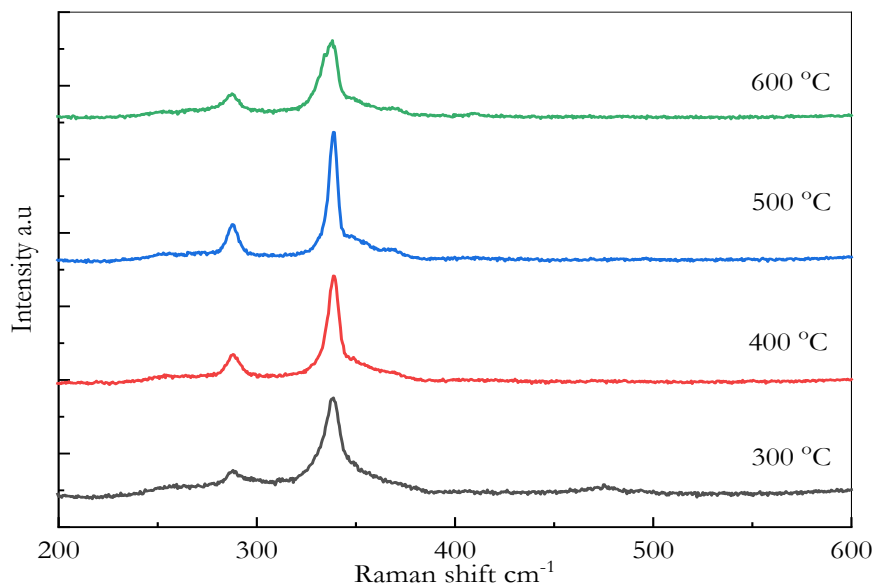

Figure 3 Raman measurements of CZTS films annealed at different temperatures 300, 400, 500 and 600 ^{o}C.

Figure 4 shows the SEM images of the formation of CZTS microparticles and nanoparticles in the films demonstrating agglomeration with a non-uniform surface and an inhomogeneous size distribution of cracks. Also, samples annealed at 400 and 600 ^{o}C show some bright and large particles which could be associated with secondary phases or incorporated elements during the annealing process.

However, the image of the sample annealed at 500 ^{o}C for 1 hour appears uniform and homogeneous with small voids and cracks. Also, the grain size of particles is observed to be uniform and of nanoparticle scale, whereas other samples were largely aggregated. These particles are composed of primary crystallites with sizes larger than 1 μm. The conversion efficiency of CZTS solar cells is known to increase with an increase in the grain size of the absorber layer material. Therefore, larger grains are required for the fabrication of highly efficient solar cells. Voids and cracks in the absorber layer of the thin film solar cell leads to low conversion efficiency because the generated carriers recombine. Large grain size in the absorber layer is important to both the minority carrier diffusion length and the recombination potential in polycrystalline thin film solar cells.
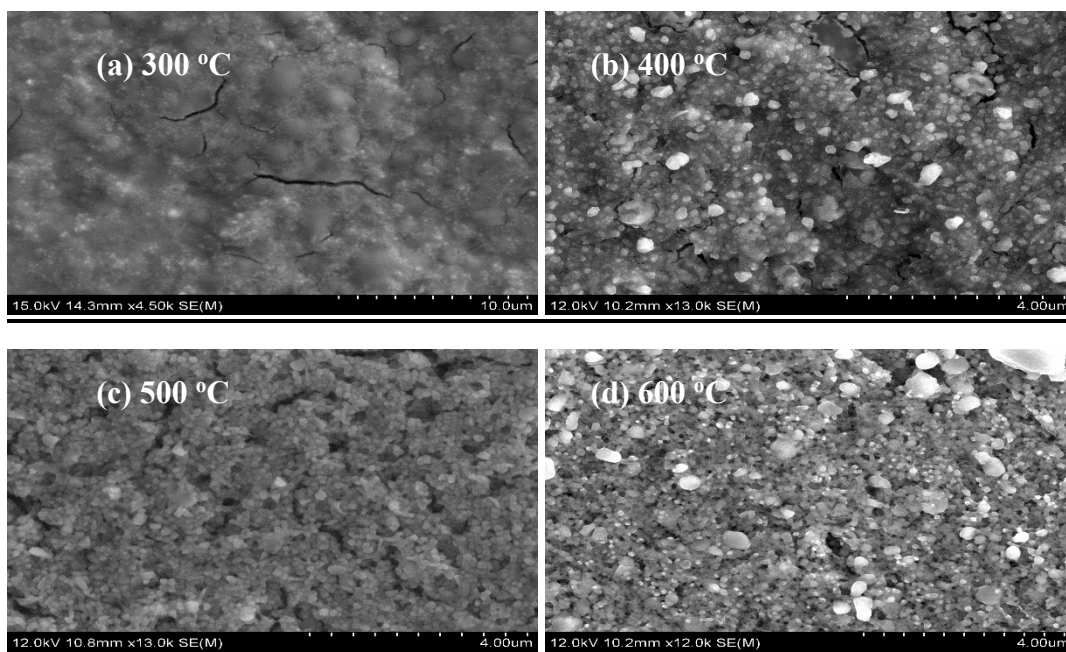
Figure 4 SEM images of CZTS thin films annealed at different temperatures (a) 300 ºC, (b) 400 ºC, (c) 500 ºC and (d) 600 ºC.

The effects of annealing temperature on CZTS compositions were studied using EDX techniques as reported in Table 1. However, the composition of Cu/(Zn+Sn), Zn/Sn and Cu/Sn show only small changes with increasing annealing temperatures except samples annealed at 600 ºC which has a big change in its composition and is close to a stoichiometric composition.

Table 1 Chemical compositions and elemental ratio of CZTS thin films prepared with different annealing temperatures.

Annealing temperature (ºC)	Composition %				Ratio			
	S	Cu	Zn	Sn	Cu/(Zn+Sn)	Zn/Sn	Cu/Sn	S/Metal
300	44.9	25.98	19.11	13.33	0.80	1.43	1.95	0.76
400	43.71	26.65	18.82	12.52	0.85	1.50	2.13	0.75
500	49.03	23.96	15.39	12.18	0.87	1.26	1.97	0.97
600	48.77	24.89	11.63	11.4	1.04	1.02	2.01	1.02

It can be seen in Table 1 that the relative composition of Zn and Sn decreased with increasing annealing temperatures, leading to a decreasing Zn/Sn ratio except for the sample annealed at 400 ºC. Moreover, samples annealed at 300 and 400 ºC have insufficient sulphur content, whereas samples annealed at 500 and 600 ºC have sufficient sulphur content. As previous results have shown, controlling the element ratio in CZTS plays an important role on CZTS crystal structure and therefore on high efficiency solar cells devices. It is known that CZTS solar cells with high efficiency were produced under Cu poor and Zn rich compositions; we achieved this condition by sample annealing at 500 ºC in N_2 atmosphere.

3.2 Annealing effect over different time period

X-ray diffraction and Raman measurements confirm that all samples annealed over different time periods are highly crystalline. In x-ray diffraction, shown in Figure 5, all high intensity peaks at 18.6, 28.6, 33.3, 47.5, 56.7 and 69.8° match well with CZTS pattern reference (JCPDS card 26-0575) corresponding to the kesterite structure. Also, the peak intensity of films increases with increasing annealing time which is due to the improvement of the crystallinity of the CZTS thin films.
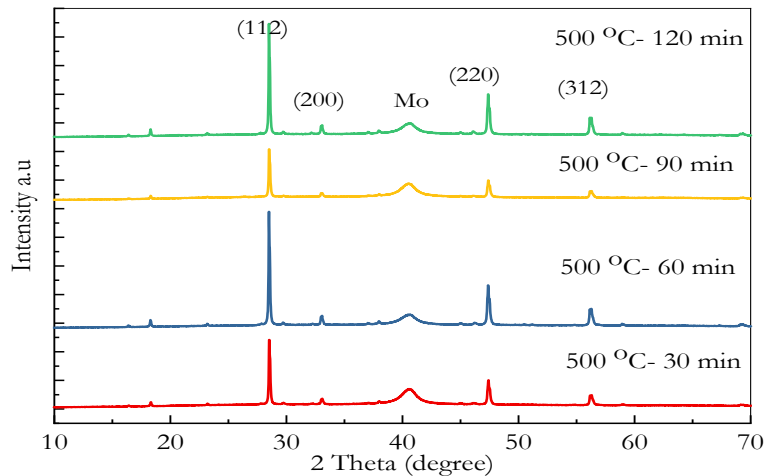

Figure 5 X-ray diffraction of CZTS films annealed at different times 30, 60, 90 and 120 min at 500 °C.

The Raman measurements were preformed using a 532 nm excitation source. The high resolution Raman spectra of the CZTS samples under different annealing times show the strong peak at 338 cm^{-1}, which is associated with vibrations of sulphur atoms, and three weak peaks at 287, 352 and 370 cm^{-1} as shown in Figure 6.

Raman modes of CZTS have been reported with high intensity peaks in the range 333-339 cm^{-1} and low intensity peaks at 145, 165, 250-255, 286-289, 350-357, 360-365 and 370-375 cm^{-1} [19-21]. These shifts in frequency are due to disorder in the Cu and Zn cations in the kesterite structure of CZTS thin films [22]. Also, the shape and position of intense peaks is affected by defects in the material [23, 24].
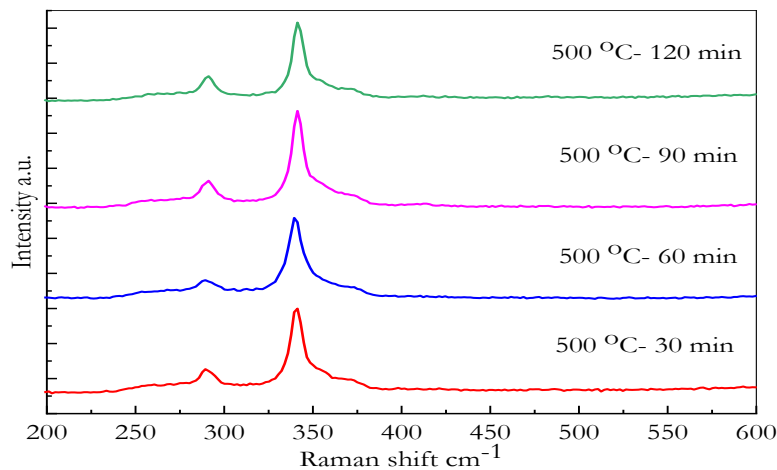

Figure 6 Raman measurements of CZTS films annealed at different times 30, 60, 90 and 120 min at 500 °C.

However, the high intensity peaks in the range 335-337 cm^{-1} may also be assigned to a tetragonal CTS phase [17, 21], but the absence of its other two low shoulder peaks expected at 297 cm^{-1} and 351 cm^{-1} [23, 25] rule out this phase being assigned. The weak peak at 304 cm^{-1} may be assigned to cubic-CTS or Sn_2S_3 phase in accordance with the reported data [17, 19, 26, 27].

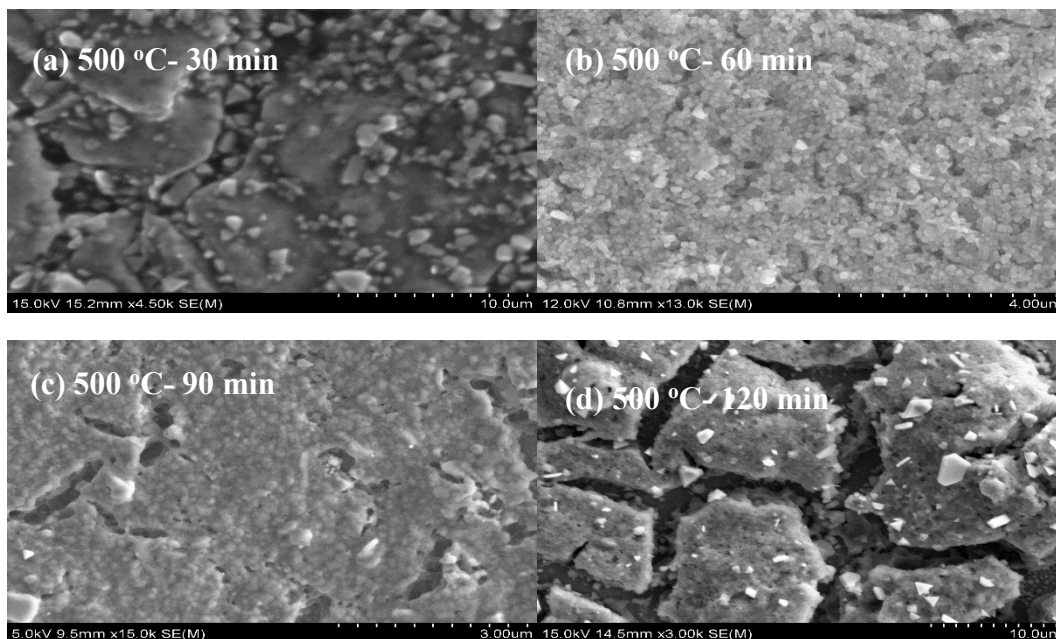SEM images in Figure 7 show the CZTS surface following different annealing times, 30, 60, 90 and 120 minutes, under an N_2 atmosphere at 500 °C.

Figure 7 SEM images of CZTS thin films annealed at different times, (a) 30 (b) 60 (c) 90 and (d) 120 minutes at 500 °C.

It can be seen that annealing for long times leads to numerous cracks in the surface with the CZTS particles developing larger sizes in the range of micrometres. Also, annealing at 2 hours showed a small bright particle which may correspond to secondary phases having different shapes, whereas annealing for 30 minutes showed some cracks in the surface with various shapes and sizes of particles. Annealing at 90 minutes also showed some cracks with holes in the surface and merger of some small particles together with a number of larger particles in some regions of the film's surface. However, the sample annealed for 60 minutes showed the most uniform distribution of particles with regular shapes and sizes having CZTS particles of nanometre scale, but with some pinholes in the surface. This demonstrates that the crystallinity has improved, leading to the formation of a dense morphological structure. Table 2 shows the atomic per cent composition and ratios of Cu/(Zn + Sn), Cu/Zn, Zn/Sn, and S/(Cu + Zn + Sn) for CZTS thin films as functions of the annealing time for 30, 60, 90 and 120 minutes at a temperature of 500 °C determined by EDX measurements. Annealing at different times shows no significant changes in the S and Cu during the annealing process. However, the Zn and Sn elemental composition decrease with increasing annealing times because of the higher vapour pressure of Zn and Sn during annealing at 500 °C.

Table 2 Chemical compositions and element ratios of CZTS thin films prepared under different annealing times at a temperature of 500 °C.

Annealing time (min)	Composition %				Ratio			
	S	Cu	Zn	Sn	Cu/(Zn+Sn)	Zn/Sn	Cu/Sn	S/Metal
30	48.08	24.31	15.59	13.06	0.85	1.19	1.86	0.91
60	49.03	23.96	15.39	12.18	0.87	1.26	1.97	0.95
90	49.51	24.54	12.39	11.41	1.03	1.09	2.15	1.02
120	49.55	24.35	11.17	10.71	1.11	1.04	2.27	1.07

Our data shows that during longer annealing times the ratios of Cu/(Zn+Sn), Cu/Sn and S/Metal increased with increasing annealing time with the films becoming stoichiometric at 90 minutes and Cu rich at 120 minutes, whereas the Zn/Sn ratio decreased with increasing annealing times which leads to changes in the film composition from Cu-poor Zn-rich to nearly stoichiometric and Cu-rich compositions. However, this change in the elemental compositions may affect the CZTS device optical and electrical properties. For instance, Cu-rich CZTS thin films can assist the formation of passivated defect clusters such as (Cu_{Zn} + Sn_{Zn}) and ($2Cu_{Zn}$ + Sn_{Zn}) which produce a deep donor level in the band gap and hence reduce the band gap of CZTS. However, Zn-rich films are necessary to form Zn_{Sn} acceptors and reduce the presence of Sn_{Zn} donors which leads to an increase in the conductivity of CZTS thin films [28-30].

3.3 Annealing effect under different ramping rates

X-ray diffraction and Raman measurements were performed to study the effects of different annealing ramping rates of 5, 10, 15, 20 °C/min, on CZTS structure. X-ray diffraction is shown in Figure 8 and confirms sharp peaks located at 28.3, 33.2, 47.5 and 56.2° which can be attributed to the diffraction pattern of (112), (200), (220) and (312) planes of the CZTS kesterite structure (JCPDS card 26-0575). There are no additional peaks which can be attributed to secondary phases in any samples except the sample annealed at 15 °C/min. In this sample, annealed at 15 °C/min, there is an additional peak located at 46.4° which corresponds to the secondary phase Cu_2S [31]. The overall diffraction patterns confirm that the ramping rate has little effect on the CZTS thin film structures.
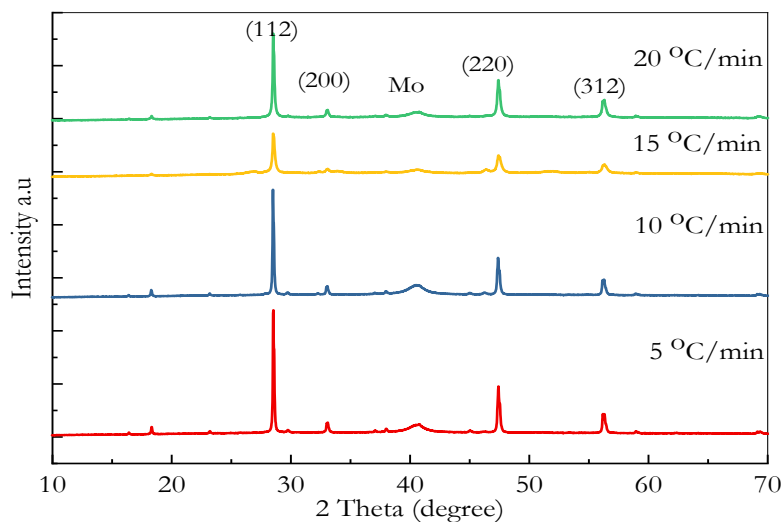

Figure 8 X-ray diffraction of CZTS films annealed at different ramping rates 5, 10, 15 and 20 °C/min.

In order to identify possible secondary phases, Figure 9 shows the Raman spectra for all samples. Each sample has an intense peak at 338 cm^{-1} with other weaker peaks at 255, 289, 360 and 370 cm^{-1}. These are identified as the main vibrational A1 mode for single phase CZTS. Also, there is a small peak at 310 cm^{-1} which can be attributed to the Cu_2SnS_3, secondary phase. The presence of the five major CZTS peaks in the Raman spectra confirms the formation of the CZTS phase. In addition, the sharp and relatively intense major peak indicates good crystalline quality of CZTS thin films.

The ZnS secondary phase Raman peaks located at 271 cm^{-1} and 352 cm^{-1} were not observed which further confirms the formation of a good quality single phase CZTS. Also, there is no evidence for $Cu_{2-x}S$ secondary phase at 475 cm^{-1} [18, 25, 32-34].
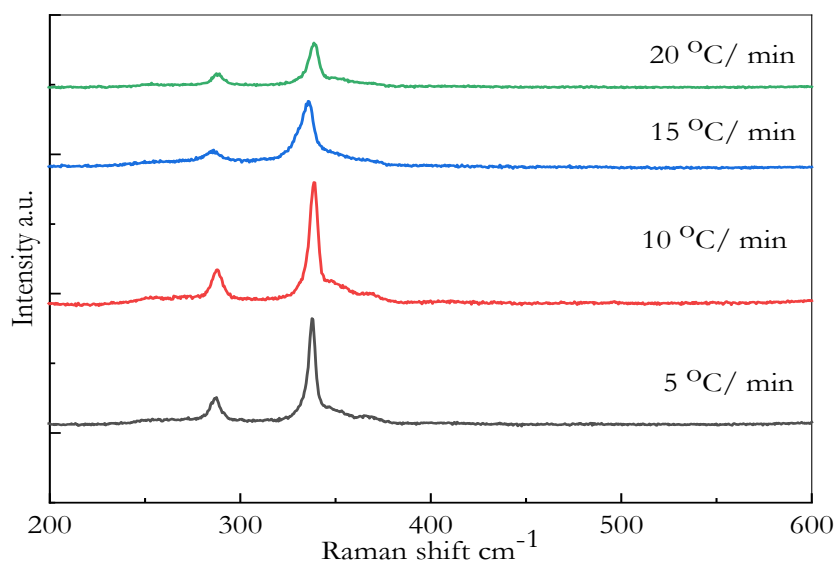

Figure 9 Raman measurements of CZTS films annealed at different ramping rates 5, 10, 15 and 20 °C/min.

The SEM images for samples annealed under different ramping rates are presented in Figure 10. These show that the samples annealed at 15 and 20 °C/min have a small number of bigger micron sized particles. Those annealed at 5 °C/min have smaller particles. The sample annealed at 10 °C/min has the most uniform distribution of particles of both shape and size. The diameter of the largest particles of CZTS are up to 2 μm. Also, the size of the smallest particles show no big change with different ramping rates. However, the faster ramping rate of 15 °C/min produces more cracks and holes on the surface of the CZTS film.

In detail, annealing at low ramping rates, 5 °C/min, showed some large particles with different sizes as revealed in Figure 10(a). Annealing at fast ramping rates of 15 and 20 °C/min showed a highly nonuniform distribution of size and shape of CZTS particles in Figures 10(c) and 10(d). However, the most uniform film produced by annealing at 10 °C/min improved the crystallinity compared with other ramping rates as shown in Figure 10(b). The ratio of CZTS elements Cu/(Zn + Sn) was 0.91 for the ramping rates at 5 and 15 °C/min, 0.93 for the ramping rate at 20 °C/min and 0.87 for the 10 °C/min ramping rate as shown in Table 3. The ratio of Zn/Sn was 1.68, 1.26, 1.48 and 1.13 for 5, 10, 15 and 20 °C/min ramping rates respectively. This provides confirmation that all samples have Cu-poor and Zn-rich compositions. A Cu-poor condition leads to the formation of Cu vacancies which generate shallow acceptors in CZTS, whereas a Zn-rich condition suppresses the Cu substitutions at Zn sites, which increases deep acceptors. Recent studies indicate that Cu-poor and Zn-rich CZTS films have higher p-type conductivity and result in high efficiency solar cells [28, 35, 36].
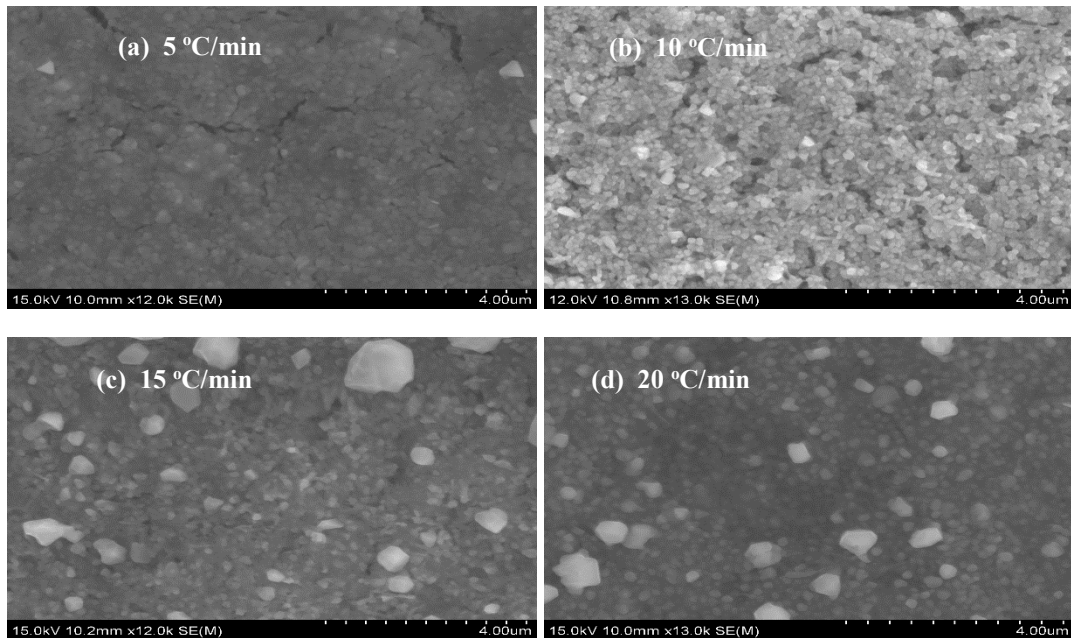
Figure 10 SEM images of CZTS thin films annealed at different ramping rates, (a) 5 ºC/min, (b) 10 ºC/min, (c) 15 ºC/min and (d) 20 ºC/min.

Table 3 Chemical compositions and element ratios of CZTS thin films prepared with different annealing ramping rates.

Annealing rate ºC/min	Composition %				Ratio			
	S	Cu	Zn	Sn	Cu/(Zn+Sn)	Zn/Sn	Cu/Sn	S/Metal
5	47.32	25.68	17.62	10.47	0.91	1.68	2.45	0.88
10	49.03	23.96	15.39	12.18	0.87	1.26	1.97	0.95
15	47.33	24.96	16.41	11.07	0.91	1.48	2.25	0.90
20	48.52	24.37	13.85	12.27	0.93	1.13	1.99	0.96

3.4 Annealing effect under different atmospheres

In order to study the effect of the annealing atmosphere (N_2, H_2S+N_2 20:80) on CZTS film properties, x-ray diffraction, Raman spectroscopy, SEM and EDX measurements were carried out. In x-ray diffraction measurements, shown in Figure 11, there are four main peaks at 28.5º, 33.0º, 47.4º and 56.3º corresponding to the (112), (200), (220), and (312) planes of CZTS which match the kesterite structure (JCPDS card 26-0575). There were no peaks related to secondary phases observed in x-ray diffraction, however binary or ternary sulphides such as ZnS, $Cu_{2-x}S$, and Cu_2SnS_3 have similar diffraction patterns with CZTS owing to their similar zinc blend-type structures [36]. It is found that the particle size of CZTS nanoparticles is significantly altered by the annealing atmosphere, this can be seen as the splitting in all peaks disappears under the H_2S+N_2 atmosphere where the size of particles is found to be close to 60 nm.
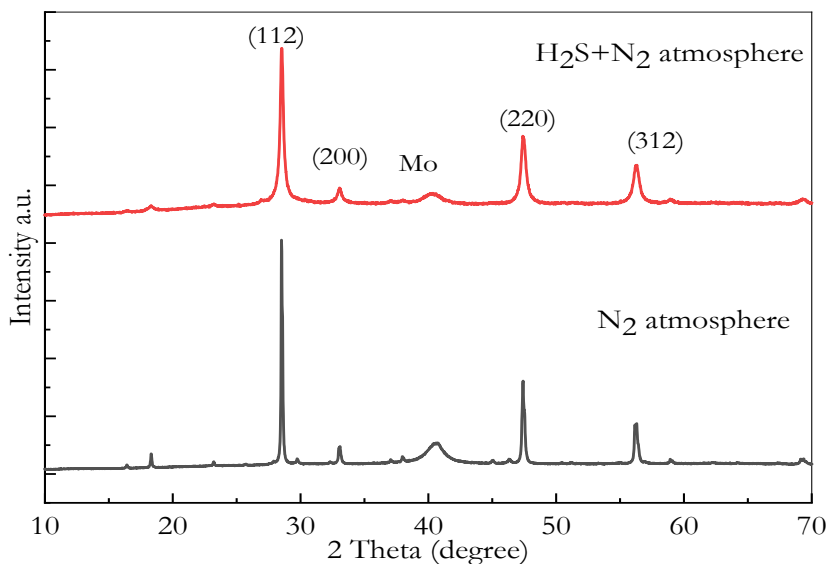
Figure 11 X-ray diffraction of CZTS films annealed in different H_2S+N_2 and N_2 atmospheres.

Raman measurements shown in Figure 12 confirm that the main CZTS Raman peak of films fabricated under different annealing atmospheres was located at 338 cm^{-1}. Also, other small peaks observed at 287, 335, 352 and 366 cm^{-1}, in both samples and correspond to a single CZTS phase. The spectra confirm that there are no additional peaks arising from secondary phases as discussed above.
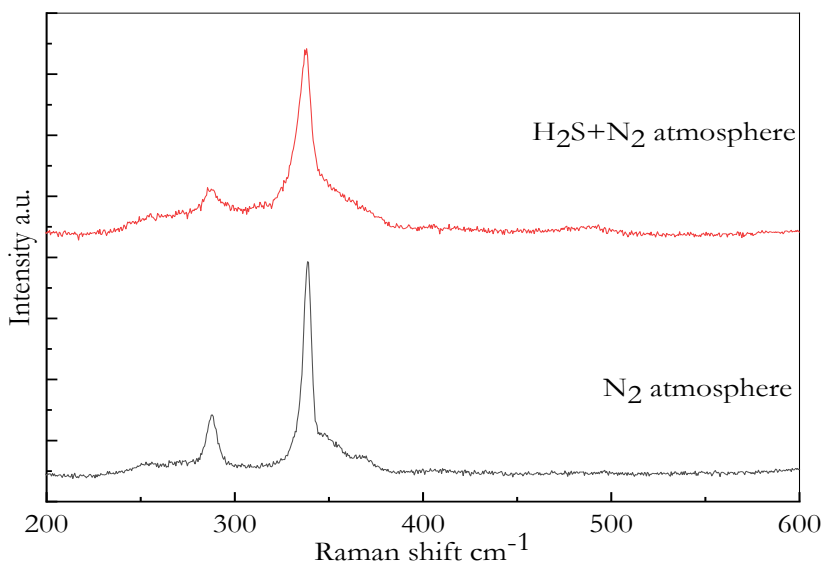

Figure 12 Raman measurements of CZTS films annealed under different atmospheres H_2S+N_2 20:80 and N_2.

The surface morphology of the films was observed by SEM. Figure 13 shows the CZTS film images of the samples annealed under different atmospheres. The film annealed at 500 ºC for 1 h with 10 ºC/min under N_2 atmosphere shows a polycrystalline film structure with some region of particles having dispersed grains with different size distributions. Also, the surface shows some cracks and holes. A similar trend is observed in the sample annealed under the H_2S+N_2 atmosphere; here the size distribution is more uniform with holes in some areas of the film surface. Overall the film surface is smoother and more continuous for this sample.
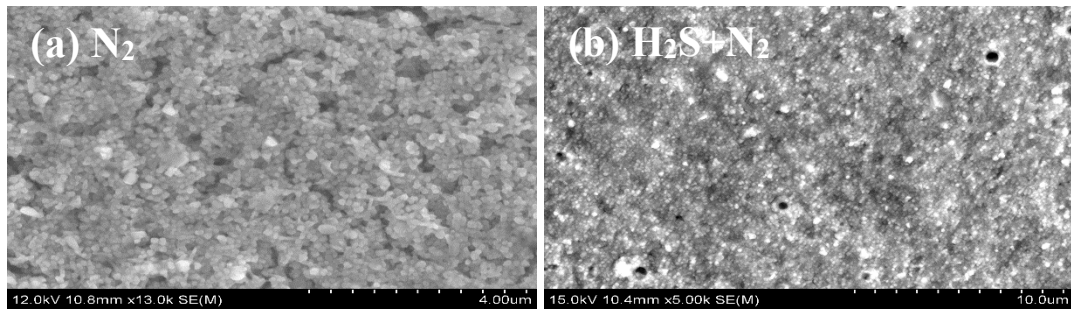
Figure 13 SEM images of CZTS thin films annealed under different atmospheres (a) N_2 atmosphere and (b) H_2S+N_2 atmosphere

EDX studies showed the content of Cu, Zn and Sn decreased with the S content increasing when annealed under a H_2S+N_2 atmosphere, leading to a ratio of S/metal of above one which provides a good indication that the sulfurisation process is completed. Table 4 shows the composition of the films under different annealing atmospheres. These are found to be Cu-poor and Zn-rich which are favourable for high efficiency solar cells.

Table 4 Chemical compositions and element ratios of CZTS thin films prepared with different annealing atmospheres.

Annealing atmosphere	Composition %				Ratio			
	S	Cu	Zn	Sn	Cu/(Zn+Sn)	Zn/Sn	Cu/Sn	S/Metal
N_2	49.03	23.96	15.39	12.18	0.87	1.26	1.97	0.95
H_2S+N_2	51.22	21.95	13.88	10.92	0.89	1.27	2.01	1.09

4 Conclusion

The CZTS nanoparticles were fabricated successfully using the hot injection method and thin films subsequently deposited using spin coating techniques. The aims of this study were to investigate the influence of the annealing parameters: temperature, length of time, ramping rate and annealing atmosphere on CZTS thin films' structure and optical properties. A range of techniques were used to analyse the prepared films. The x-ray diffraction in all samples show the main peaks at 28.5°, 33.2°, 47.5° and 56.4° which corresponds to kesterite, stannite or disordered kesterite structures. It is difficult to distinguish between all these structures because the deviation between them is small. However, the Raman measurements confirm the presence of single phase CZTS thin films with the main Kesterite vibrational mode at 338 cm^{-1} with other weaker Kesterite Raman peaks at 335 cm^{-1}. Also, the intensity of x-ray diffraction peaks and Raman peaks increased and become sharper with increased annealing conditions (temperature, time and ramping rate) with improvements in the CZTS crystallinity. SEM was used to study the surface of CZTS films and showed uniformly distributed films. An EDX study indicated that the chemical composition ratio of Cu/(Zn+Sn), Zn/Sn, Cu/Sn and S/Metal was affected by the annealing parameters and all ratios were observed to be greater than the initial compositions due to Zn and Sn losses during the annealing process. The mapping image shows the homogeneous distribution of CZTS elements which is one of the important requirements for CZTS thin film solar cells. The crystallinity, structure and chemical composition of CZTS thin films increased and improved under annealing in an H_2S+N_2 20:80 atmosphere. It was concluded that annealing at 500 ºC for 1 hour with 10 ºC/min ramping rate under an H_2S+N_2 20:80 atmosphere at 0.15 atm is a suitable condition for CZTS thin film formation for use in high efficiency solar cell devices.

Acknowledgements

5 References

1. Wang, K., et al., *Thermally evaporated Cu₂ZnSnS₄ solar cells.* Applied Physics Letters, 2010. **97**(14): p. 3.
2. Shin, B., et al., *Thin film solar cell with 8.4% power conversion efficiency using an earth-abundant Cu₂ZnSnS₄ absorber.* Progress in Photovoltaics, 2013. **21**(1): p. 72-76.
3. Khalkar, A., et al., *Effect of Growth Parameters and Annealing Atmosphere on the Properties of Cu₂ZnSnS₄ Thin Films Deposited by Cosputtering.* International Journal of Photoenergy, 2013.
4. Fukano, T., S. Tajima, and T. Ito, . Applied Physics Express, 2013. **6**(6): p. 3.
5. Guo, Q., et al., *Fabrication of 7.2% Efficient CZTSSe Solar Cells Using CZTS Nanocrystals.* Journal of the American Chemical Society, 2010. **132**(49): p. 17384-17386.
6. Guo, Q., H.W. Hillhouse, and R. Agrawal, *Synthesis of Cu₂ZnSnS₄ Nanocrystal Ink and Its Use for Solar Cells.* Journal of the American Chemical Society, 2009. **131**(33): p. 11672-11673.
7. Raiguru, J., et al., *Impact of Annealing Temperature on the Phase of CZTS with the Variation in Surface Morphological Changes and Extraction of Optical Bandgap*, in *National Conference on Processing and Characterization of Materials*. 2017, IOP Publishing Ltd: Bristol.
8. Bahramzadeh, S., H. Abdizadeh, and M.R. Golobostanfard, *Controlling the morphology and properties of solvothermal synthesized Cu₂ZnSnS₄ nanoparticles by solvent type.* Journal of Alloys and Compounds, 2015. **642**: p. 124-130.
9. Zhou, B., D. Xia, and Y. Wang, *Phase-selective synthesis and formation mechanism of CZTS nanocrystals.* RSC Advances, 2015. **5**(86): p. 70117-70126.
10. Ahmad, R., et al., *A comprehensive study on the mechanism behind formation and depletion of Cu2ZnSnS4 (CZTS) phases.* CrystEngComm, 2015. **17**(36): p. 6972-6984.
11. Chernomordik, B.D., et al., *Rapid facile synthesis of Cu₂ZnSnS₄ nanocrystals.* Journal of Materials Chemistry A, 2014. **2**(27): p. 10389-10395.
12. Khare, A., et al., *Calculation of the lattice dynamics and Raman spectra of copper zinc tin chalcogenides and comparison to experiments.* Journal of Applied Physics, 2012. **111**(8): p. 9.
13. Kumar, M., et al., *Strategic review of secondary phases, defects and defect-complexes in kesterite CZTS-Se solar cells.* Energy & Environmental Science, 2015.
14. Dimitrievska, M., et al., *Multiwavelength excitation Raman scattering study of polycrystalline kesterite Cu₂ZnSnS₄ thin films.* Applied Physics Letters, 2014. **104**(2).
15. Wang, Z.R., S. Elouatik, and G.P. Demopoulos, *Understanding the phase formation kinetics of nano-crystalline kesterite deposited on mesoscopic scaffolds via in situ multi-wavelength Raman-monitored annealing.* Physical Chemistry Chemical Physics, 2016. **18**(42): p. 29435-29446.
16. Sun, R.J., et al., *Cu₂ZnSnSSe₄ solar cells with 9.6% efficiency via selenizing Cu-Zn-Sn-S precursor sputtered from a quaternary target.* Solar Energy Materials and Solar Cells, 2018. **174**: p. 42-49.
17. Fernandes, P.A., P.M.P. Salomé, and A.F. da Cunha, *Study of polycrystalline Cu2ZnSnS4 films by Raman scattering.* Journal of Alloys and Compounds, 2011. **509**(28): p. 7600-7606.
18. Patel, K., et al., *Cu₂ZnSnS₄ thin-films grown by dip-coating: Effects of annealing.* Journal of Alloys and Compounds, 2016. **663**: p. 842-847.
19. Wang, K.J., et al., *Structural and elemental characterization of high efficiency Cu₂ZnSnS₄ solar cells.* Applied Physics Letters, 2011. **98**(5): p. 3.
20. Yoo, H. and J. Kim, *Growth of Cu₂ZnSnS₄ thin films using sulfurization of stacked metallic films.* Thin Solid Films, 2010. **518**(22): p. 6567-6572.
21. Fontané, X., et al., *In-depth resolved Raman scattering analysis for the identification of secondary phases: Characterization of Cu₂ZnSnS₄ layers for solar cell applications.* Applied Physics Letters, 2011. **98**(18): p. 181905.
22. Caballero, R., et al., *Cu₂ZnSnS₄ thin films grown by flash evaporation and subsequent annealing in Ar atmosphere.* Thin Solid Films, 2013. **535**: p. 62-66.

23.   Chalapathi, U., S. Uthanna, and V.S. Raja, *Growth of Cu2ZnSnS4 thin films by co-evaporation-annealing route: effect of annealing temperature and duration.* Journal of Materials Science-Materials in Electronics, 2018. **29**(2): p. 1048-1057.

24.   Valakh, M.Y., et al., *Optically induced structural transformation in disordered kesterite Cu_2ZnSnS_4.* JETP Letters, 2013. **98**(5): p. 255-258.

25.   Fernandes, P.A., P.M.P. Salome, and A.F. da Cunha, *A study of ternary Cu_2SnS_3 and Cu_3SnS_4 thin films prepared by sulfurizing stacked metal precursors.* Journal of Physics D-Applied Physics, 2010. **43**(21).

26.   Fernandes, P.A., P.M.P. Salome, and A.F. da Cunha, *Growth and Raman scattering characterization of Cu_2ZnSnS_4 thin films.* Thin Solid Films, 2009. **517**(7): p. 2519-2523.

27.   Kumar, S., et al., *Study of CZTS nano-powder synthesis by hot injection method by variation of Cu and Zn concentrations*, in *Proceedings of the 2016 E-MRS Spring Meeting Symposium T - Advanced Materials and Characterization Techniques for Solar Cells III*, S. Yerci, et al., Editors. 2016. p. 136-143.

28.   Chen, S.Y., et al., *Intrinsic point defects and complexes in the quaternary kesterite semiconductor Cu_2ZnSnS_4.* Physical Review B, 2010. **81**(24).

29.   Ruan, C.-H., et al., *Electrical properties of $Cu_xZn_ySnS_4$ films with different Cu/Zn ratios.* Thin Solid Films, 2014. **550**: p. 525-529.

30.   Yeh, M., C. Lee, and D. Wuu, *Influences of synthesizing temperatures on the properties of Cu_2ZnSnS_4 prepared by sol–gel spin-coated deposition.* Journal of Sol-Gel Science and Technology, 2009. **52**(1): p. 65-68.

31.   Mkawi, E., et al., *Dependence of Copper Concentration on the Properties of Cu_2ZnSnS_4 Thin Films Prepared by Electrochemical Method.* Int. J. Electrochem. Sci, 2013. **8**: p. 359-368.

32.   Pawar, S.M., et al., *Synthesis of Cu_2ZnSnS_4 (CZTS) absorber by rapid thermal processing (RTP) sulfurization of stacked metallic precursor films for solar cell applications.* Materials Letters, 2014. **118**: p. 76-79.

33.   El Kissani, A., et al., *Synthesis, annealing, characterization, and electronic properties of thin films of a quaternary semiconductor; copper zinc tin sulfide.* Spectroscopy Letters, 2016. **48**(5): p. 343-347.

34.   Nguyen, D.C., S. Ito, and D.V.A. Dung, *Effects of annealing conditions on crystallization of the CZTS absorber and photovoltaic properties of Cu(Zn,Sn)(S,Se)(2) solar cells.* Journal of Alloys and Compounds, 2015. **632**: p. 676-680.

35.   Chen, S., et al., *Crystal and electronic band structure of Cu_2ZnSnX_4 (X=S and Se) photovoltaic absorbers: First-principles insights.* Applied Physics Letters, 2009. **94**(4).

36.   Park, H., Y.H. Hwang, and B.-S. Bae, *Sol-gel processed Cu_2ZnSnS_4 thin films for a photovoltaic absorber layer without sulfurization.* Journal of Sol-Gel Science and Technology, 2013. **65**(1): p. 23-27.